Colloids and Surfaces B: Biointerfaces 114 (2014) 96–103

Contents lists available at ScienceDirect

Colloids and Surfaces B: Biointerfaces

journal homepage: www.elsevier.com/locate/colsurfb

Biofunctional quantum dots as fluorescence probe for cell-specific targeting☆

Didem Ag[a], Rebecca Bongartz[b], Leyla Eral Dogan[c], Muharrem Seleci[a], Johanna-G. Walter[b], Dilek Odaci Demirkol[a], Frank Stahl[b], Serdar Ozcelik[c], Suna Timur[a,*], Thomas Scheper[b]

[a] Ege University, Faculty of Science, Department of Biochemistry, 35100 Bornova-Izmir, Turkiye
[b] Leibniz University of Hannover, Institute for Technical Chemistry, Callinstr. 5, 30167 Hannover, Germany
[c] Izmir Institute of Technology, Department of Chemistry, Faculty of Science, 35430 Urla-Izmir, Turkiye

ARTICLE INFO

Article history:
Received 4 June 2013
Received in revised form
14 September 2013
Accepted 16 September 2013
Available online 4 October 2013

Keywords:
Quantum dots
Anti-HER2
Bioconjugation
Cell specific targeting
Imaging

ABSTRACT

We describe here the synthesis, characterization, bioconjugation, and application of water-soluble thioglycolic acid TGA-capped CdTe/CdS quantum dots (TGA-QDs) for targeted cellular imaging. Anti-human epidermal growth factor receptor 2 (HER2) antibodies were conjugated to TGA-QDs to target HER2-overexpressing cancer cells. TGA-QDs and TGA-QDs/anti-HER2 bioconjugates were characterized by fluorescence and UV–Vis spectroscopy, X-ray diffraction (XRD), hydrodynamic sizing, electron microscopy, and gel electrophoresis. TGA-QDs and TGA-QDs/anti-HER2 were incubated with cells to examine cytotoxicity, targeting efficiency, and cellular localization. The cytotoxicity of particles was measured using an MTT assay and the no observable adverse effect concentration (NOAEC), 50% inhibitory concentration (IC_{50}), and total lethal concentration (TLC) were calculated. To evaluate localization and targeting efficiency of TGA-QDs with or without antibodies, fluorescence microscopy and flow cytometry were performed. Our results indicate that antibody-conjugated TGA-QDs are well-suited for targeted cellular imaging studies.

1. Introduction

Cancer is one of the leading causes of death worldwide. Early detection of tumor cells can prevent approximately 3.0% to 35% of cancer deaths; thus, it is essential that imaging probes be developed for the early diagnosis of cancer [1,2]. Functionalized fluorescent nanoparticles, such as quantum dots (QDs), are promising probes for biomedicine and cancer research [3,4]. As fluorescent probes, QDs are fundamentally different from organic dyes [5]. Although successful cell labeling has been achieved with organic dyes, they are plagued by low quantum yields and photobleaching. QDs overcome many these problems due to their excellent physical and fluorescent properties [6], including broad absorption spectra, narrow emission spectra [7,8], high quantum yields, resistance to photobleaching, and high photochemical stability [9,10]. Therefore, biocompatible QDs are ideal for cell-labeling studies [11].

Because of the large surface area of QDs, they are readily modified with surface-conjugated biomolecules and proteins [12–14]. QDs are commonly used to image tumor cells after surface labeling with peptides, antibodies, or receptor ligands, such as folate [15]. Guan et al. characterized transferrin-conjugated CdTe/CdSe QDs by different methods and evaluated their cellular targeting capabilities [16]. In another study, RNase-A-associated CdTe QD clusters were coupled to monoclonal antibodies against the human epidermal growth factor receptor 2 (HER2). These theranostic QDs were then used to image and treat gastric cancer *in situ* in a mouse model [17]. Yu et al. reported using GSH-TGA-QDs-ND-1 probes that specifically react with the LEA antigen to target colorectal cancer cells [18]. Geszke-Moritz et al. evaluated the accumulation of folate-conjugated, thioglycerol-capped, Mn-doped ZnS QDs and their subsequent cytotoxicity in T47D breast cancer cells [19]. Recently, Liu et al. synthesized water-soluble indium phosphide/ZnS QDs (QInP) that were functionalized with carboxyl groups and polyethylene glycol (PEG). QinP were then loaded into cells with cell-penetrating peptides (CPP) [20].

Biomedical applications require water-soluble QDs [21]. However, QDs are typically produced in organic solvents, making them

* Corresponding author. Tel.: +902323112455, fax: +902323115485.
E-mail addresses: suna.timur@ege.edu.tr, sunatimur@yahoo.com (S. Timur).

0927-7765/$ – see front matter © 2013 The Authors. Published by Elsevier B.V. All rights reserved.
http://dx.doi.org/10.1016/j.colsurfb.2013.09.033

unsuitable for direct use in biological studies [22]. For cell imaging, the QDs must be transferred into aqueous solutions using ligand exchange reactions, and then conjugated to relevant biomolecules before being incubated with cells [23,24]. Pretreatments, such as ligand exchange, increase the size of QDs, which can make them impracticable for *in vitro* applications [25]. By modification with hydrophilic surface moieties that interact with the aqueous phase, QDs can be rendered water soluble without any additional modification [26].

Antibodies are commonly used targeting moieties because of their diversity and high specificity [27]. For cell imaging, QDs have been modified with cell-targeting antibodies against various antigens, such as the epidermal growth factor receptor (EGFR) [26], Rh-interferon [28], and HER2 [29]. Lung cancer cells often overexpress the erbB (HER) family of oncogenes [30,31]. The c-erbB2 gene encoding the HER2 protein is expressed in 20–30% of non-small cell lung cancers (NSCLCs) and, especially, adenocarcinoma [31,32].

The objective of the study was to design and synthesize fluorescent probes for cell-targeting studies. Water-soluble, thioglycolic acid (TGA)-capped QDs (TGA-QDs) were labeled with anti-HER2 antibodies to specifically image HER2-positive A549 lung cancer cells. Due to the carboxyl groups present on TGA-capped QDs, a simple reaction using 1-ethyl-3-(3-dimethylaminopropyl)carbodiimide (EDC) and *N*-hydroxysuccinimide (NHS) conjugated antibodies to QDs. Expression of the HER2 receptor in A549 cells and NIH-3T3 control cells was confirmed by PCR and flow cytometry. Targeting specificity of the TGA-QD/anti-HER2 conjugates was characterized by several methods. Finally, the cellular internalization of QDs was visualized by fluorescence microscopy.

2. Materials and methods

2.1. Materials

All chemicals used here were of the highest purity available. Cadmium chloride ($CdCl_2$, 99%) was ordered from Fluka. Thioglycolic acid (TGA, $HSCH_2CO_2H$, 98%) was purchased from Merck. Tellurium precursor (NaHTe) was prepared from the reaction between sodium borohydride ($NaBH_4$, Riedel 95%) and tellurium powder (Te, Fluka 99.9%). Thiourea (CH_4N_2S, Aldrich 99.5%) was the sulfur source for CdS shell formation. 2-Propanol (C_3H_8O, Riedel 99.5%) was used to purify the nanoparticles. All precursor solutions were prepared using ultra-pure water as a solvent. Rabbit monoclonal antibody against human HER2 protein was obtained from Diagnostic Biosystems. 2-(*N*-morpholino) ethanesulfonic acid (MES), 1-ethyl-3-(3-dimethylaminopropyl) carbodiimide hydrochloride (EDC), *N*-hydroxysuccinimide (NHS), 3-(4,5-dimethylthiazol-2-yl)-2,5-diphenyl tetrazoliumbromide (MTT), 4,6-diamino-2-phenylindol (DAPI) and Dulbecco's Modified Eagle Medium (DMEM) were ordered from Sigma Aldrich. Sodium dodecyl sulfate (SDS) and RNAtidy G were purchased from Applichem. Phosphate-buffered saline (PBS) was prepared with 137 mM sodium chloride, 2.7 mM potassium chloride, 10.1 mM disodium hydrogen phosphate and 1.8 mM potassium dihydrogen phosphate, pH 7.4; all chemicals were provided from Sigma Aldrich. The chemicals for protein expression analysis, chloroform, ethanol (75%) and the ingredients of Tris-acetate-EDTA buffer (TAE) that consists of 40 mM 2-Amino-2-(hydroxymethyl)-1,3-propanediol (tris-base), 20 mM glacial acetic acid and 1.0 mM ethylenediaminetetraacetic acid (EDTA), pH 8.0 were purchased from Sigma Aldrich. $Oligo(dT)_{12-18}$ Primer, agarose and Roti-Safe GelStain were ordered from Carl Roth GmbH (Karlsruhe, Germany). The dNTP Set (100 mM solutions) and GeneRuler 100 bp DNA Ladder were obtained from Fermentas. M-MLV reverse transcriptase and its M-MLV RT 5× buffer as well as GoTaq polymerase and its 5× Green GoTaq reaction buffer were provided from Promega (Mannheim, Germany). PCR primers were synthesized by life technologies. Chemicals for native PAGE experiment, ammoniumpersulfate (APS), tetramethylenediamine (TEMED), tris–hydrochloric acid, glycine and bromophenol blue were obtained from Sigma Aldrich. Forty percent acrylamide/bisacrylamide mixing ratio, 37.5:1 was purchased from Carl Roth GmbH. Glycerol was ordered from Fluka.

2.2. Synthesis of water soluble TGA-QDs

In a typical synthesis of CdTe QDs a modified one pot method from the literature was used [33]. Both Te^{2-} and Cd^{2+} precursors were prepared separately. Sodium hydrogen telluride (NaHTe) was prepared by reduction of Te powder with sodium borohydride ($NaBH_4$). Te powder (0.0918 g) and $NaBH_4$ (0.06 g) were put into 25 mL reaction flask and it was purged with N_2 for 30 min. Then 10 mL of deaerated distilled water was added to the reaction flask and the system was heated to 60 °C for 2 h under N_2 atmosphere to obtain a solution with a purple color.

3.12 mmols of $CdCl_2$ and 420 μL of thioglycolic acid were dissolved in 110 mL of ultra-pure water in a two-necked flask with a septum. pH of the solution was adjusted to 11.0–11.5 by drop wise addition of NaOH solution (1.0 M). Then the flask was attached to the condenser under N_2 for an hour at 80 °C to purge oxygen in the medium. The reflux time was one hour. Further reflux before the addition of Te^{2-} precursor may cause decomposition of thioglycolic acid to give S^{2-} [34]. Then 2.5 mL freshly synthesized NaHTe (Te^{2-} precursor) was added to the solution and the reaction temperature was increased to 110 °C.

Formation and growth steps are proceeding upon reflux. As soon as the temperature reaches to 110 °C, sampling was started to observe the growth of the particles. After 10 min, the solution emitted green light under UV-irradiation.

To increase the photostability of the nanoparticles, CdTe NCs were coated with CdS shell. CdS is preferred as a shell material for CdTe cores because band gap of CdS (2.5 eV) is wider than that of CdTe (1.5 eV) and also lattice parameter mismatch between CdTe and CdS is about 3.6% [35].

Proper amount of thiourea dissolved in ultra-pure water was added to green emitting CdTe QDs. The ratio of Te:S related to the amount of applied Te was optimized to 1:10. After addition of thiourea solution, reflux was continued. The prolonged reflux results in red-shifting in both UV–Vis and fluorescence spectra upon coating are indication of core/shell structure formation rather than $CdTe_xS_{1-x}$ alloyed structure. CdTeS alloy structure has larger band gap energy than CdTe and the alloy formation will cause blue-shifting rather than red-shifting. By a changing reflux time, proper sized QDs can be prepared.

2.3. Characterization of TGA-QDs

The synthesized QDs were characterized both optically and structurally. UV–Vis Spectrometer and fluorescence spectrophotometer were used for characterization of optical properties of the nanocrystals. Fluorescence and absorbance spectra of QDs were measured with Varian Cary Eclipse fluorescence spectrophotometer and Varian Cary 50 UV–Vis absorption spectrophotometer. Quantum yield of emission from the QDs is defined as ratio of number of emitted photons to absorbed photons by the QDs. Experimentally the quantum yield can be calculated by absorption and fluorescence emission spectra by comparing fluorescence of both unknown substance and a dye of known quantum yield [36]. Quantum yield of emission from the QD's were measured by using Rhodamine 6G in water as a standard (the reference quantum

yield of 0.95).Structural characterization of the nanoparticles was done by X-Ray Diffractometry (XRD), and transmission electron microscopy (TEM). X-ray powder diffraction patterns of the QDs were obtained by using a Philips X'pert Pro X-ray diffractometer. The grounded samples were placed on a zero-background silicon sample holder. Data was collected by using CuK_α ($\lambda = 1.5406$ Å) radiation at settings of −45 kV and 40 mA for 45 min. The scan rate was 0.1/sn and the data was collected for 2θ values of 5.0 to 60. TEM images were taken by using JEOL microscope. For the analyses, a drop of QD solution was placed onto a copper grid surface and dried at room temperature. The samples were placed onto the holder then given to the microscope and images were acquired using a voltage of 200 kV.

2.4. Preparation of TGA-QDs bioconjugate

TGA-QDs/anti-HER2 conjugates were prepared as follows: 2.0 M EDC and 0.5 M NHS were separately prepared in 25 mM (pH 6.0) MES buffer. A volume of 200 μL QDs solutions (0.91 mg/mL) were mixed with 25 μL EDC and 25 μL NHS at room temperature to activate carboxyl groups of TGA-QDs. Then, anti-HER2 antibody was added and reaction was completed in 4 h at room temperature. Finally, the bioconjugates were purified using 300 kDa membrane filter (Sartorius Stedim Biotech) and washed with PBS three times.

2.5. Characterization of TGA-QDs bioconjugate

To verify the successful preparation of bioconjugates both a native PAGE and agarose gel were used. Samples of conjugates and pure quantum dots were separated in 2.0% agarose gel in TAE buffer at 98 V for 15 min by Thermo EC electrophoresis unit. Therefore 30 μL of samples were mixed with 10 μL two-fold loading dye, consisting of 23.9 M formamide, 0.867 mM SDS, 0.373 mM bromophenol blue, 0.464 mM xylenecyanol, 0.5 mM EDTA. For the native PAGE, 15% running gel was prepared using 1875 μL 40% acrylamide/bisacrylamide (37.5:1), 500 μL bidistilled water, 1400 μL Tris–HCl (1.5 M, pH 8.8), 1225 μL bidistilled water, 10 μL TEMED and 10 μL APS. 6.0% stacking gel was prepared using 750 μL 40% acrylamide/bisacrylamide (37.5:1), 300 μL bidistilled water, 630 μL Tris–HCl (0.5 M, pH 6.8), 3770 μL bidistilled water, 10 μL TEMED and 10 μL APS. For preparation of running buffer 3.63 g Tris and 15.96 g glycine were added in 600 mL water and adjust to pH 8.9. Samples of conjugates and pure anti-HER2 antibody were added in 20 μL sample buffer including 5.0 mL glycerol, 2.7 mL water, 2.13 mL Tris–HCl (0.5 M, pH 6.8) and a trace amount bromophenol blue. Gel was run by using mini Protean III electrophoresis unit (Bio-Rad) at 30 mA/100 V. Finally, the gel was stained with silver. For the characterization of sizes, samples were diluted 1:10 with PBS (pH 7.4) and the hydrodynamic diameters of QDs and TGA-QDs/anti-HER2 conjugates were evaluated by using dynamic light scattering (DLS, Malvern Zetasizer Nanoseries-Nano-ZS). Fluorescence spectra of TGA-QDs/anti-HER2 conjugates were measured with Varian Cary Eclipse fluorescence spectrophotometer and by using 2.0 μL of sample for Nanodrop 3300 spectrofluorometer (Thermo Fisher Scientific Inc. USA) in terms of relative fluorescence units (RFU). The effect of conjugation on the fluorescence characteristics of QDs was examined according to the fluorescence spectrum. Photostability of TGA-QDs/anti-HER2 was tested via measuring fluorescence intensity of conjugates for 30 days, stored at 4 °C in the dark.

The Bradford protein assay was used for the analysis of protein content in the bioconjugate using Coomassie Brilliant Blue G-250 by following of the optical densities at 595 nm. The protein concentration of the sample is determined by comparison to that of a series of BSA standards. The amount of bound anti-HER2 in the QD bioconjugate was then calculated. A microplate reader (Thermo Labsystems Multiscan Spectrum) was used for the analysis.

2.6. Cell line

A549 (human lung cancer) and NIH-3T3 (mouse fibroblast) cell lines were provided from German Collection of Microorganisms and Cell Cultures (DSMZ). Cell culture supplies including fetal calf serum (FCS Gold), Newborn Calf Serum (NCS) and penicillin/streptomycin (P/S, 100×) were purchased from PAA Laboratories GmbH. A549 cells were grown in DMEM containing 10% FCS and 1.0% P/S. NIH-3T3 cells were cultivated in DMEM containing 10% NCS and 1.0% P/S. All cells were cultivated in medium and incubated with samples and reagents at 37 °C in humidified environment with 5.0% CO_2.

2.7. HER2 expression on cell surfaces

Expression of the HER2 receptor in A549 and lack of expression in NIH-3T3 cells as control cell line was first confirmed by PCR and flow cytometry analysis. Therefore, total cellular RNA of 2×10^6 cells was isolated, transcribed into cDNA and used for PCR following the same procedures as described in our earlier publication [37]. The PCR primer pair for the c-erbB2 gene was designed with Lasergene PrimerSelect Software using the NCBI reference mRNA sequence for homosapiens v-erbB2 erythroblastic leukemia viral oncogene homolog 2 (homo sapiens erbB2, NM_001005862.1). The primer sequences are as followed: erbB2 human forward 5′tgc ggc tcg tac aca ggg act t3′, reverse 5′tgc ggg aga att cag aca cca act3′. To verify the success of reverse transcription a primer pair for the human housekeeping gene hypoxanthine phosphoribosyltransferase (HPRT) and the mouse housekeeping gene glyceraldehyde-3-phosphate dehydrogenase (GAPDH) were additionally used. The primer sequences are: HPRT forward 5′-aag ctt gct ggt gaa aag ga-3′ and reverse 5′-aag cag atg gcc aca gaa ct-3′, as well as GAPDH forward 5′-aac ttt ggc att gtg gaa gg-3′ and reverse 5′-aca cat tgg ggg tag gaa ca-3′. The polymerase chain reactions was performed using the protocol described in our earlier publication[24], but for erbB2 expression analysis 2.0 μL cDNA and 31.75 μL distilled autoclaved water were used. For expression analysis of c-erbB2 an annealing temperature of 64 °C, for HPRT of 60 °C and for GAPDH of 58 °C were used. Products of PCR were separated in 1.5% agarose gel in TAE buffer stained with 5.0 μL/100 mL buffer Roti-Safe GelStain ready-to-use by Thermo EC electrophoresis unit at 100 V for 60 min. The gel was documented using an INTAS UV documentation system. For flow cytometry studies, the same procedure as previously described [37] was used. For staining of 5×10^5 cells 0.04 μg mouse IgG1 anti-human HER2-FITC antibody, clone Neu 24.7 (BD Biosciences, Heidelberg) were added and cell suspension was shaken at room temperature for 1 h with 500 rpm in the dark. As negative control cells were stained using mouse IgG1, k FITC isotype control antibody (BD Biosciences, Heidelberg). The stained cells were analyzed in a COULTER EPICS XL-MCL flow cytometer. At least 10 000 gated events were observed in total and living cells were gated in a dot plot of forward versus side scatter signals. For drawing dot plots and histograms the software WinMDI 2.9 was used.

2.8. Cytotoxicity

3-(4,5-Dimethylthiazol-2-yl)-2,5-diphenyl tetrazolium bromide (MTT) assays were used to determine dose dependent cytotoxicity of TGA-QDs and bioconjugates. Cells were seeded out in 96-well-tissue plates (Sarstedt, USA) in a volume of 200 μL. The cultivation took three days at 37 °C, 5.0% CO_2 and 100% air humidity. After this cultivation time the wells were grown until reaching confluence. A549 and NIH-3T3 cells were washed once in

PBS and treated with TGA-QDs and TGA-QDs/anti-HER2 conjugates at 5, 10, 20, 30, 60, 120, 180 and 240 μg/mL concentrations for 2 h. Then the samples were removed completely and cells were incubated in 110 μL/well 10% MTT solution (5.0 mg/mL PBS) in supplements-free medium for 4 h. With this incubation time the formazan complex was produced inside the cells. To release the purple coloured salt, 100 μL SDS solution (1.0 g SDS in 10 mL 0.01 M HCl) were added per well and after 24 h of incubation, UV–Vis absorption was measured at 570 nm with 630 nm as reference wavelength using a microplate reader Model 680 (BioRad).

2.9. Cellular uptake study by flow cytometry

For flow cytometry studies the cells were harvested by accutase treatment, washed once in ice-cold PBS and incubation buffer consisting of PBS supplemented with 2.0% FCS. Then 3×10^5 cells in incubation buffer were collected and centrifuged. For cell staining 40 μg/mL TGA-QDs/anti-HER2 conjugates were added and cell suspension was shaken at room temperature for 1 h with 450 rpm in the dark. Cells were washed once in 500 μL incubation buffer to remove unbound conjugates. Before flow cytometric analysis cells were suspended in 300 μL incubation buffer and then analyzed in a COULTER EPICS XL-MCL flow cytometer. The analysis of measured signals was done as described above.

2.10. Fluorescence microscopy

A549 and NIH-3T3 cells were cultivated for three days on glass chamber slides (Nunc) in a volume of 200 μL medium until 80% confluence was reached. TGA-QDs/anti-HER2 conjugates and TGA-QDs were diluted with medium and 100 μL of samples (60 μg/mL) were added to the cells. The cells were incubated for 2 h at 37 °C and were washed twice in PBS. Afterwards cell's nuclei were counterstained by DAPI solution (1.0 μg/mL) for 15 min and cells were washed again twice in PBS. Conjugate-labelled cells were covered with fluoroshield (Carl Roth) and imaged using Olympus BX53F fluorescence microscope equipped with a CCD camera (Olympus DP72). For QDs fluorescence a U-MNB excitation filter, BP470-490 (exciter filter), BA515 (barrier filter) and for DAPI fluorescence a U-MWU excitation filter, BP330-385 (exciter filter), BA420 (barrier filter) were used. To figure out if the internalization process is driven by endocytotic pathways, cells were stained as described before, but incubated at a temperature of 4 °C.

3. Results and discussion

3.1. Characterization of QDs

QDs with CdTe cores and CdS shells exhibited a diffraction pattern similar to that of bulk cubic CdTe. The crystal structure of CdTe/CdS QDs was a zincblende type. The XRD pattern of the QDs resembled the general pattern of the cubic lattice. The diffraction peaks shifted to larger angles, which were between those of cubic CdTe and CdS crystals. The peak locations between CdTe and CdS crystals indicated formation of a CdS shell (Fig. 1A).

The mean particle size was 5.4 ± 1.8 nm according to dynamic light scattering (DLS) (Malvern Zetasizer). The diameter was confirmed to be ~5.0 nm by transmission electron microscopy (TEM) (Fig. 1B). The normalized absorbance and fluorescence spectra of QDs are shown in Fig. S1. Emission wavelengths of CdTe/CdS QDs were tuneable by adjusting the reaction times. Yellow-emitting QDs were used (λ_{em} = 560 nm) during the experiments and the quantum yield of emission from the QDs was ~36% at an excitation wavelength of 488 nm.

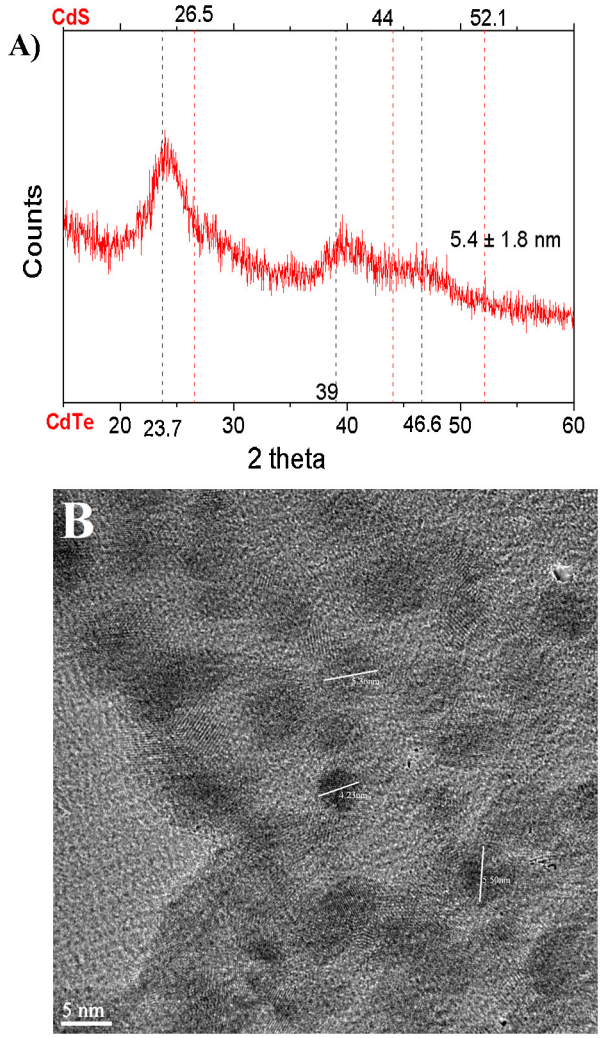

Fig. 1. (A) XRD pattern of CdTe/CdS QDs. Blue lines show 2 theta of face centered cubic bulk CdTe (bottom), red lines represent the 2 theta of face centered cubic bulk CdS (top), (B) TEM images of CdTe/CdS core shell QDs, scale bar: 5.0 nm. (For interpretation of the references to color in this figure legend, the reader is referred to the web version of this article.)

3.2. Characterization of TGA-QD bioconjugates

Different methods have been used to conjugate antibodies to carboxy-functionalized QDs [23,38]. We conjugated anti-HER2 antibodies to TGA-QDs using EDC/sulfo-NHS coupling reactions that covalently linked antibodies to TGA-QDs. During this process, NHS was used as an activating agent for carboxyl groups on the TGA-QDs. NHS formed amide linkages to amines on antibodies. Gel electrophoresis in 2.0% agarose and polyacrylamide was used to verify antibody conjugation qualitatively. The antibody-conjugated QDs appeared to be heavier upon electrophoresis than QDs, demonstrating conjugation (Fig. 2A). DLS, TEM, and Bradford assays were performed to characterize the antibody-conjugated QDs. The hydrodynamic diameter increased to 14.33 ± 2.0 nm after bioconjugation (Fig. 2B). Protein content was determined using Bradford assays, which compared experimental values to a bovine serum albumin (BSA) standard curve ($y = 1.2214x + 0.0028$, $R^2 = 0.9943$). The starting amount of antibody was 3.925 μg. After conjugation, TGA-QDs were washed with PBS to remove unbound antibodies, and the binding efficiency was determined to be 50%.

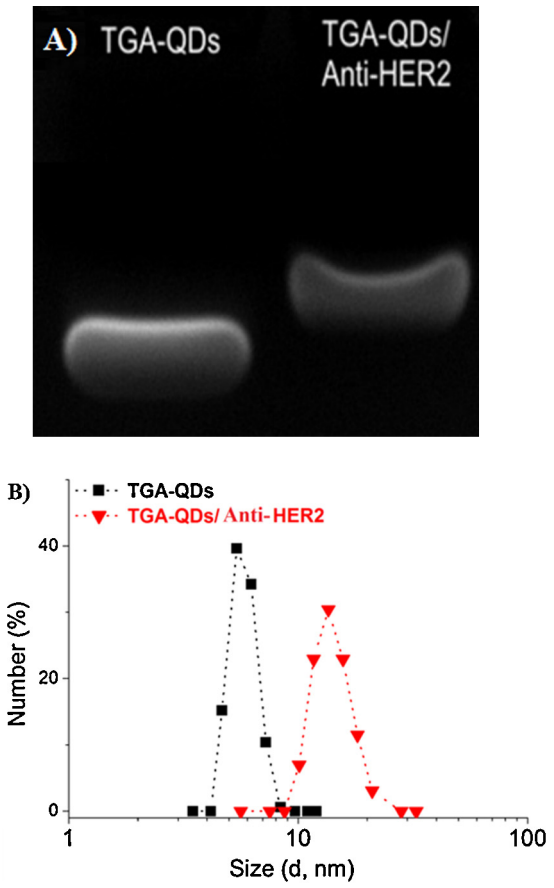

Fig. 2. Confirmation of conjugation of TGA-QDs with anti-HER2 (A) 2.0% agarose gel (B) hydrodynamic diameters of TGA-QDs and TGA-QDs/anti-HER2.

The amount of antibody conjugated to TGA-QDs was 10.67 μg of protein per 1 mg of QDs.

The potential effects of antibody conjugation on the fluorescence characteristics of TGA-QDs were measured by fluorescence spectroscopy. Antibody conjugation reduced the fluorescence intensity of TGA-QDs, but did not shift the emission wavelength. Overall, antibody conjugation did not dramatically affect the fluorescent properties of TGA-QDs (Fig. S3).

3.3. Photostability

QDs must be photostable for cell-imaging experiments. Due to their high photostability, similar QDs have been successfully used for *in vivo* tumor targeting studies [39]. Byrne showed that QDs are suitable for cell imaging studies because of their high photostability [40]. We measured the photostability of TGA-QDs/anti-HER2 conjugates stored in the dark at 4 °C and measured their fluorescence intensity for 30 days. Stored under these conditions, QDs remained fluorescent for 30 days without any significant decrease in fluorescence.

3.4. HER2 expression on cell surfaces

To test QDs as cellular imaging probes, we measured cellular HER2 expression using polymerase chain reaction (PCR) and HER2 expression on cell surfaces using flow cytometry. The PCR results are shown in Fig. 3. The housekeeping gene hypoxanthine phosphor-ribosyltransferase (HPRT) was measured as a control for A549 cells, and glyceraldehyde-3-phosphate dehydrogenase (GAPDH) served as the control for NIH-3T3 cells (Fig. S4). Bands corresponding to housekeeping genes were observed for both cell types (263 bp for A549 cells and 224 bp for NIH-3T3 cells). Fig. 3A shows a HER2 band at 420 bp in A549 cells that is absent in NIH-3T3 cells.

The PCR results were also confirmed at the protein level by using fluorescently labeled antibodies and flow cytometry. The flow cytometry results using at least 10 000 cells per measurement are shown in Fig. 3. Cells were incubated with a fluorescein isothiocyanate (FITC)-labeled mouse IgG1 isotype as a negative control or a FITC-labeled mouse HER2 antibody. Partial image S5 figures out the fluorescence measurement of NIH-3T3 cells and Fig. 3B shows the signals of A549 cell line. The mean intensity of isotype controls for NIH-3T3 cells was 2.7 AU, whereas the isotype control for A549 was 1.9 AU. The mean fluorescence intensity after incubating with the anti-HER2 antibody was 2.7 AU for NIH-3T3 cells, but 6.9 AU for A549 cells. Both methods confirmed that HER2 expression was considerably higher in A549 cells than in NIH-3T3 cells.

3.5. Cytotoxicity

The cytotoxicity of Cd-based QDs is thought to occur from released Cd^{2+} ions [41]. Using QDs with shells or coatings minimizes Cd^{2+} release from the particle surface [42]. Su et al. demonstrated that uncoated CdTe QDs are toxic to cells, but coating the surface

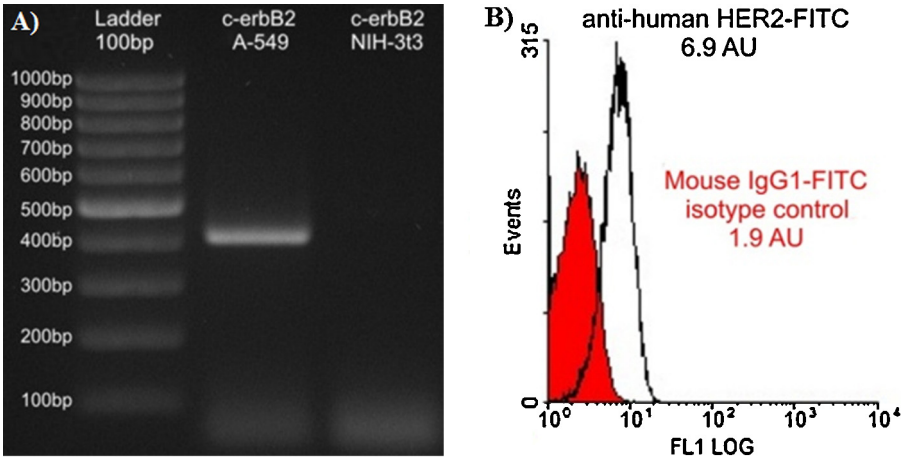

Fig. 3. (A) For c-erbB2 expression in A549 and NIH-3T3 cells. (B) A549 cell characterization for HER2 protein expression via flow cytometry, red: Cells incubated with IgG-FITC negative control, black: Cells stained with anti-human HER2-FITC. Measured relative fluorescence intensities are given as numbers. (For interpretation of the references to color in this figure legend, the reader is referred to the web version of this article.)

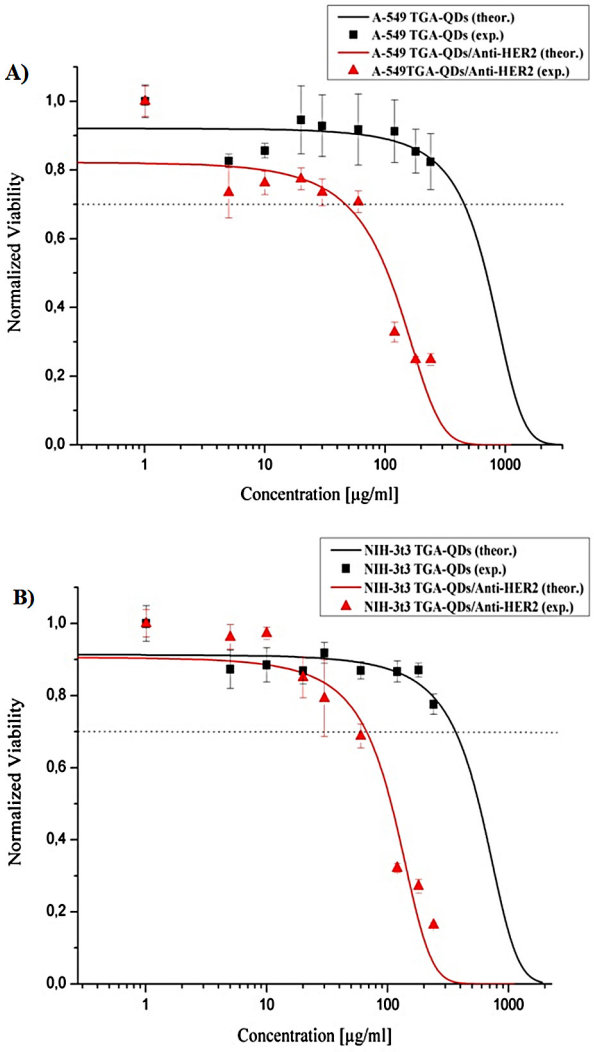

Fig. 4. (A) Dose dependent cytotoxic effects on viability of A549 (B) NIH-3T3 cells (Black curve: Cells incubated with TGA-QDs, red curve: Cells incubated with TGA-QDs/anti-HER2, black dot line represents point of significant cytotoxicity (70% viability). Values are the mean ± standard deviation of the data ($N = 4$). (For interpretation of the references to color in this figure legend, the reader is referred to the web version of this article.)

with a CdS layer reduces toxicity [43]. To evaluate the dose-dependent cytotoxic effects of our QD preparations, the viability of NIH-3T3 and A549 cells were determined using a standard MTT assay. NIH-3T3 and A549 cells were incubated with anti-HER2 TGA-QDs or TGA-QDs alone for 2 h at different concentrations, and cell viability was measured (Fig. 4). A cytotoxic effect was observed for both cell lines incubated with TGA-QDs/anti-HER2; however, TGA-QDs alone did not show significant cytotoxicity. It is possible that the increase in cytotoxicity was caused by interactions between the TGA-QDs/anti-HER2 and the cells, which is consistent with previous findings [44].

Cytotoxicity data obtained from MTT assays were extrapolated using the exponential equation ($y = 1 - (1/(1 + e^a \times (b - x))))$, where a is the slope, b is IC_{50} (50% inhibitory concentration) and x is the concentration of sample. Also, the no observable adverse effect concentration (NOAEC) and total lethal concentration (TLC) were calculated using similar equations. Estimated toxicity values in terms of IC_{50}, NOAEC, and TLC are shown in Table S1. The IC_{50} values of TGA-QDs/anti-HER2 conjugates is approximately were similar for A549 cells (IC_{50} = 105.4 μg/mL) and NIH-3T3 cells (IC_{50} = 107.1 μg/mL), but ~6 times lower than the IC_{50}

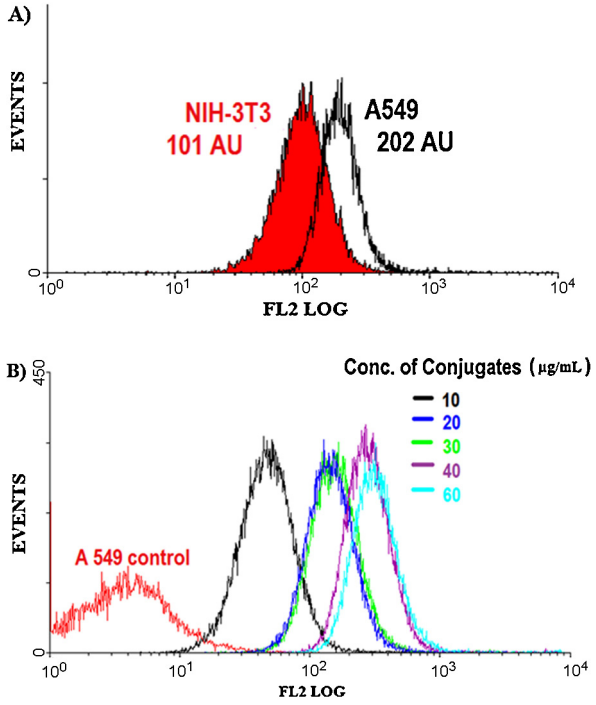

Fig. 5. (A) Histogram of specific binding of TGA-QDs/anti-HER2 to HER2-negative NIH-3T3 cells and HER2-positive A549 cells (B) concentration-dependent binding of TGA-QDs/anti-HER2 to A549 cells.

values for unconjugated TGA-QDs (IC_{50} = 696.7 μg/mL for A549; IC_{50} = 569.4 μg/mL for NIH-3T3).

3.6. Cellular targeting and uptake

To confirm the binding specificity of anti-HER2 TGA-QDs, they were incubated with A549 and NIH-3T3 cells. After incubation with anti-HER2 TGA-QDs, the fluorescence intensity of A549 cells was ~2-fold greater than NIH-3T3 cells (Fig. 5A). These results demonstrate that TGA-QDs/anti-HER2 conjugates bind to A549 cells in greater numbers than they do to NIH-3T3 cells. Caused by a high fluorescence intensity of the conjugated QDs, the measured fluorescence signal is increased, in comparison to the FITC fluorochrome used as staining dye for cell characterization (compare Fig. 3). Fig. 5B shows the relationship between the concentration of TGA-QDs/anti-HER2 and labeling of A549 cells. Greater concentrations of TGA-QDs/anti-HER2 resulted in greater fluorescence intensities. Maximal fluorescence values were measured at TGA-QDs/anti-HER2 concentrations between 40 and 60 μg/mL. For further experiments, 60 μg/mL TGA-QDs/anti-HER2 conjugate was used.

Fluorescence microscopy of internalized TGA-QDs and TGA-QDs/anti-HER2 was performed after incubating QDs with A549 cells for 2 h at 37 °C or 4 °C (Fig. 6 and S6). Modifying the QD surface with antibodies allows cellular uptake through endocytosis [45]. Fig. 6 and Fig. S6 show that TGA-QDs/anti-HER2 was endocytosed into cells by receptor-mediated endocytosis. Incubating cells at 4 °C blocks endocytosis [9]. Images of QDs incubated with A549 cells at 4 °C are shown in Fig. 6 and Fig. S7.

Nabiev et al. used TGA-capped CdTe QDs to study passive uptake by cells [46]. They showed that negatively charged TGA-capped CdTe QDs escape from endosomes and accumulate near nuclear pore complexes. We also observed that TGA-QDs accumulated in and around the nucleus (Fig. 7A and Fig. S8). When the cells were incubated with TGA-QDs at 4 °C, nanoparticles were not endocytosed (Figs. 7B and Fig. S9).

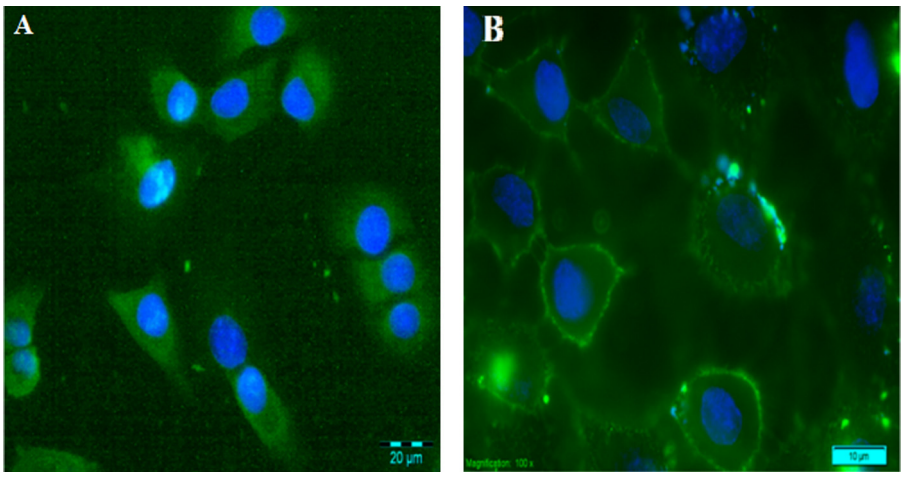

Fig. 6. Fluorescence microscopy imaging of A549 cells. Cells were treated with TGA-QDs/anti-HER2 bioconjugate for 2 h at 37 °C, (A) overlap of two images, control nuclei staining with DAPI. Cells were treated with TGA-QDs/AntiHER2 bioconjugate for 2 h at 4 °C. (B) Overlap of two images, control nuclei staining with DAPI.

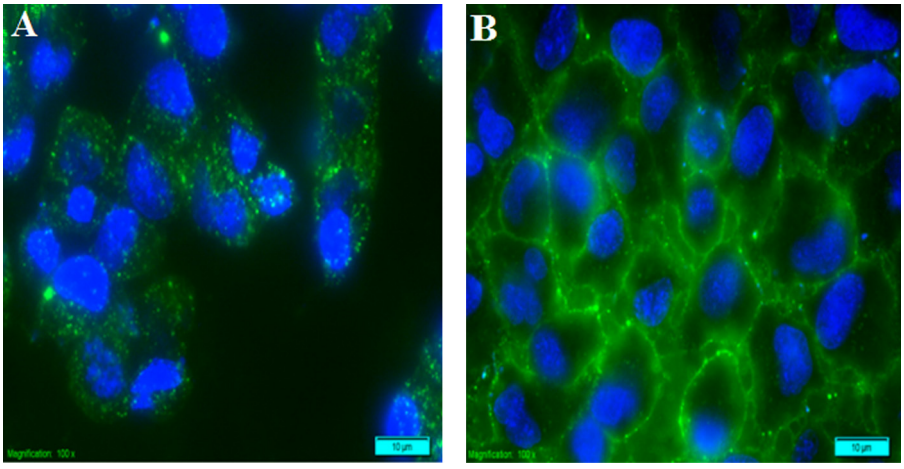

Fig. 7. Fluorescence microscopy imaging of A549 cells. Cells were treated with TGA-QDs for 2 h at 37 °C, (A) overlap of two images, control nuclei staining with DAPI. Cells were treated with TGA-QDs for 2 h at 4 °C, (B) overlap of two images, control nuclei staining with DAPI.

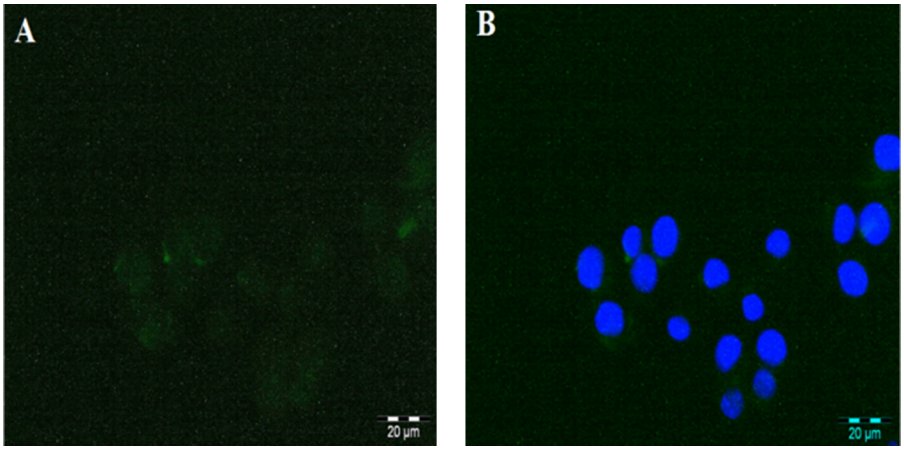

Fig. 8. Fluorescence microscopy images of NIH-3T3. (A) Cells were treated with TGA-QDs/anti-HER2 for 2 h at 37 °C, (B) overlap of two images, control nuclei staining with DAPI.

Anti-HER2 TGA-QDs nonspecifically bound to NIH-3T3 cells, but the fluorescence signals were much lower than those in A549 cells (Fig. 8A and B). The results from fluorescence microscopy were consistent with our flow cytometry results.

4. Conclusion

Water-soluble TGA-QDs were synthesized and conjugated to anti-HER2 antibodies. PCR and flow cytometry demonstrated that A549 cells expressed high levels of HER2, whereas NIH-3T3 cells did not. Antibody-conjugated TGA-QDs bound A549 cells and were endocytosed by receptor-mediated endocytosis at 37 °C. When endocytosis was blocked by incubation at 4 °C, QDs bound cells, but were not endocytosed. Cellular localization of TGA-QDs and bioconjugates were easily determined by nuclear staining, and differences in localization were clearly observed. Taken together, these results suggest that TGA-QDs/anti-HER2 can be used as fluorescent probes for cellular imaging of HER2-overexpressing cancer cells and in vivo imaging applications, such as biomarker detection.

Acknowledgement

This work is supported by Scientific and Technological Research Council of Turkey (TUBITAK, project number 109T573) and Federal Ministry of Education and Research (BMBF, project number 01DL12013). Also it was partially funded by Ege University Scientific Research Project (2012/FEN/0071). We are grateful to Michael Meyer (Gottfried Wilhelm Leibniz University of Hannover, Institute for Technical Chemistry) for his knowledge and time spent carrying out flow cytometry experiments. In addition our thanks go to F. B. Barlas (Ege University, Faculty of Science, Biochemistry department) for taking fluorescence microscope images.

Appendix A. Supplementary data

Supplementary data associated with this article can be found, in the online version, at http://dx.doi.org/10.1016/j.colsurfb.2013.09.033.

References

[1] G.A. Colditz, T.A. Sellers, E. Trapido, Nat. Rev. Cancer 6 (2006) 75.
[2] P. Suriamoorthy, X. Zhang, G. Hao, A.G. Joly, S. Singh, M. Hossu, X. Sun, W. Chen, Cancer Nano. 1 (2010) 19.
[3] S.P. Leary, C.Y. Liu, M.L. Apuzzo, Neurosurgery 58 (2006) 805.
[4] F. Pinaud, X. Michalet, L.A. Bentolila, J.M. Tsay, S. Doosel, J.J. Li, G. Iyer, S. Weiss, Biomaterials 27 (2006) 1679.
[5] H. Chen, Z. Zhen, T. Todd, P.K. Chu, J. Xie, Mater. Sci. Eng., R 74 (2013) 35.
[6] U. Resch-Genger, M. Grabolle, S. Cavaliere-Jaricot, R. Nitschke, T. Nann, Nat. Methods 5 (2008) 763.
[7] M. Bruchez Jr., M. Moronne, P. Gin, S. Weiss, A.P. Alivisatos, Science 281 (1998) 2013.
[8] W.C.W. Chan, S.M. Nie, Science 281 (1998) 2016.
[9] J.K. Jaiswal, H. Mattoussi, J.M. Mauro, S.M. Simon, Nat. Biotechnol. 21 (2003) 47.
[10] K. Hanaki, A. Momo, T. Oku, A. Komoto, S. Maenosono, Y. Yamaguchi, K. Yamamoto, Biochem. Biophys. Res. Commun. 302 (2003) 496.
[11] R.E. Bailey, A.M. Smith, S. Nie, Physica E 25 (2004) 1.
[12] Y.T. Lim, S. Kim, A. Nakayama, N.E. Stott, M.G. Bawendi, J.V. Frangioni, Mol. Imaging 2 (2003) 50.
[13] E.R. Goldman, H. Mattoussi, G.P. Anderson, I.L. Medintz, J.M. Mauro, Methods Mol. Biol. 303 (2005) 19.
[14] M. Geszke-Moritz, M. Moritz, Mater. Sci. Eng., C 33 (2013) 1008.
[15] A.M. Smith, S. Dave, S. Nie, L. True, X. Gao, Expert Rev. Mol. Diagn. 6 (2006) 231.
[16] L.Y. Guan, Y.Q. Li, S. Lin, M.Z. Zhang, J. Chen, Z.Y. Ma, Y.D. Zhao, Anal. Chim. Acta 741 (2012) 86.
[17] J. Ruan, H. Song, Q. Qian, C. Li, K. Wang, C. Bao, D. Cui, Biomaterials 33 (2012) 7093.
[18] Y. Yu, L. Xu, J. Chen, H. Gao, S. Wang, J. Fang, S. Xu, Colloids Surf., B 95 (2012) 247.
[19] M. Geszke-Moritz, H. Piotrowska, M. Murias, L. Balan, M. Moritz, J. Lulek, R. Schneider, J. Mater. Chem. B 1 (2013) 698.
[20] B.R. Liu, J.G. Winiarz, J.S. Moon, S.Y. Lo, Y.W. Huang, R.S. Aronstam, H.J. Lee, Colloids Surf., B 111 (2013) 162.
[21] W. Yu, E. Chang, R. Drezek, V.L. Colvin, Biochem. Biophys. Res. 348 (2006) 781.
[22] N. Chen, Y. He, Y. Su, X. Li, Q. Huang, H. Wang, X. Zhang, R. Tai, C. Fan, Biomaterials 33 (2012) 1238.
[23] D.K. Tiwari, S. Tanaka, Y. Inouye, K. Yoshizawa, T.M. Watanabe, T. Jin, Sensors 9 (2009) 9332.
[24] T. Liu, J.H. Wang, H.L. Zhang, Z.H. Zhang, X.F. Hua, Y.C. Cao, Y.D. Zhao, Q.M. Luo, J. Biomed. Mater. Res. 83 (2007) 1209.
[25] H.S. Choi, W. Liu, P. Misra, E. Tanaka, J.P. Zimmer, B.I. Ipe, M.G. Bawendi, J.V. Frangioni, Nat. Biotechnol. 25 (2007) 1165.
[26] L. Junghan, C. Youngseon, K. Keumhyun, H. Sukmin, P. Hye-Young, L. Taesup, C.G. Jeong, S. Rita, Bioconjugate Chem. 21 (2010) 940.
[27] J.M. Montenegro, V. Grazu, A. Sukhanova, S. Agarwal, J.M. de la Fuente, I. Nabiev, A. Greiner, W.J. Parak, Adv. Drug Delivery Rev. 65 (2013) 677.
[28] S.L. Wang, Y. Shi, H. Zhang, H. Li, H. Liu, B. Yang, T. Li, X. Fang, W. Li, Talanta 75 (2008) 1008.
[29] M. Akin, R. Bongartz, J.G. Walter, D. Odaci Demirkol, F. Stahl, S. Timur, T. Scheper, J. Mater. Chem. 22 (2012) 11529.
[30] D.H. Harpole, J.R. Marks, W.G. Richards, J.E. Herndon, D.L. Sugarbaker, Clin. Cancer Res. 1 (1995) 659.
[31] J.A. Kern, R.J. Slebos, B. Top, S. Rodenhuis, D. Lager, R.A. Robinson, D. Weinerand, D.A. Schwartz, Clin. Invest. 93 (1994) 516.
[32] M. Tateishi, T. Ishida, T. Mitsudomi, S. Kaneko, K. Sugimachi, Eur. J. Cancer 27 (1991) 1372.
[33] Z. Gu, L. Zou, Z. Fang, W. Zhu, X. Zhong, Nanotechnology 19 (2008) 135604.
[34] A.L. Rogach, T. Franzl, T.A. Klar, J. Feldmann, N. Gaponik, V. Lesnyak, A. Shavel, A. Eychmuller, Y.P. Rakovich, J.F. Donegan, J. Phys. Chem. C 111 (2007) 14628.
[35] T. Trindade, P. O'Brien, N.L. Pickett, Chem. Mater. 13 (2001) 3843.
[36] A.T.R. Williams, S.A. Winfield, J.N. Miller, Analyst 108 (1983) 1067.
[37] R. Bongartz, D. Ag, M. Seleci, J.G. Walter, E. Yalcinkaya, D. Odaci Demirkol, F. Stahl, S. Timur, T. Scheper, J. Mater. Chem. B 1 (2013) 522.
[38] Y. Xing, Q. Chaudry, C. Shen, K.Y. Kong, H.E. Zhau, L.W. Chung, J.A. Petros, R.M. O'Regan, M.V. Yezhelyev, J.W. Simons, M.D. Wang, S. Nie, Nat. Protoc. 2 (2007) 1152.
[39] L. Chen, J. Wang, W. Lib, H. Han, Chem. Commun. 48 (2012) 4971.
[40] S.J. Byrne, S.A. Corr, T.Y. Rakovich, Y.K. Gun'ko, Y.P. Rakovich, J.F. Donegan, S. Mitchell, Y. Volkov, J. Mater. Chem. 16 (2006) 2896.
[41] A.M. Derfus, W.C.W. Chan, S.N. Bhatia, Nano Lett. 4 (2004) 11.
[42] M.X. Zhao, H.F. Huang, Q. Xia, L.N. Jia, Z.W. Mao, J. Mater. Chem. 21 (2011) 10290.
[43] Y.Y. Su, Y. He, H.T. Lu, L.M. Sai, Q.N. Li, W.X. Li, L.H. Wang, P.P. Shen, Q. Huang, C.H. Fan, Biomaterials 30 (2009) 19.
[44] M. Geszke, M. Murias, L. Balan, G. Medjahdi, J. Korczynski, M. Moritz, J. Lulek, R. Schneider, Acta Biomater. 7 (2011) 1327.
[45] J.B. Delehanty, H. Mattoussi, I.L. Medintz, Anal. Bioanal. Chem. 393 (2009) 1091.
[46] I. Nabiev, S. Mitchell, A. Davies, Y. Williams, D. Kelleher, R. Moore, Y.K. Gun'ko, S. Byrne, Y.P. Rakovich, J.F. Donegan, A. Sukhanova, J. Conroy, D. Cottell, N. Gaponik, A. Rogach, Y. Volkov, Nano Lett. 7 (2007) 3452.